Experimental conditions affecting the measured fracture toughness at the microscale: Notch geometry and crack extension measurement

Ashish Kumar Saxena [a], Steffen Brinckmann [a], Bernhard Völker [b,1], Gerhard Dehm [a], Christoph Kirchlechner [a,*]

[a] Max-Planck-Institut für Eisenforschung GmbH, Max-Planck-Str. 1, D-40237 Düsseldorf, Germany
[b] Materials Chemistry, RWTH Aachen Univeristy, Kopernikusstraße 10, D-52074 Aachen, Germany

HIGHLIGHTS

- The "apparent size dependence" of the extracted elasto-plastic fracture properties is shown.
- The "apparent size dependence" is not an intrinsic material property.
- The benefits and drawbacks of Bridge notch and through thickness notch for elasto plastic fracture mechanics are identified.
- A tomographic reconstruction of crack front shows it's heterogeneity.
- Recommendations for elasto plastic fracture mechanics at the micron scale are given.

GRAPHICAL ABSTRACT
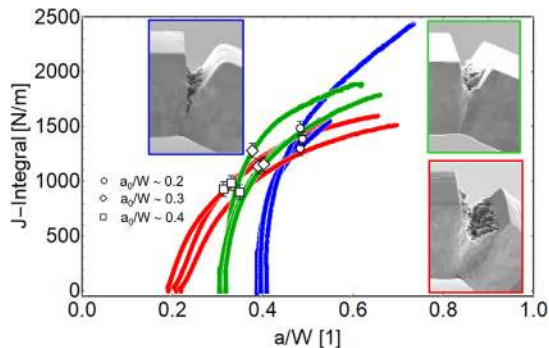
ABSTRACT

Experimental fracture mechanics at the microscale became an indispensable tool for understanding and developing advanced material systems. In case of linear elastic fracture mechanics, stringent requirements are typically only warranted for very brittle materials. The material properties of semi-brittle materials might be accessible by elasto-plastic fracture mechanics. However, challenges exist in determining the crack length, in producing geometry and notch geometry, in defining of the initiation toughness and in extracting the size independent crack resistance curves. In this study, we assess current approaches of measuring the fracture toughness of semi-brittle materials by elasto-plastic fracture mechanics. We investigate the notch geometry (through thickness notch and bridge notch), the notch depth and the method of determining *in situ* the crack length for ultrafine grained tungsten. Further challenges due to the overlap of sample size and crack process zone are identified. Finally, we propose a workflow for analyzing the elasto-plastic fracture toughness of material systems at the microscale.
© 2020 The Authors. Published by Elsevier Ltd. This is an open access article under the CC BY-NC-ND license (http://creativecommons.org/licenses/by-nc-nd/4.0/).

1. Introduction

The continuous trend of device miniaturization and shrinking component length scales has forced the scientific community to understand the mechanical properties of materials at ever smaller length scales [1–4]. Today, a complimentary toolbox of various small scale testing protocols, which are all based on nanoindentation [5] and focus ion beam (FIB) milling, exist [1,2]. The advantage of testing at the

* Corresponding author at: Karlsruhe Institute of Technologie, Institute for Applied Materials, Hermann-von-Helmholtz-Platz 1, D-76344 Eggenstein-Leopoldshafen, Germany.
E-mail address: christoph.kirchlechner@kit.edu (C. Kirchlechner).
[1] Now at: Materials Center Leoben Forschung GmbH, Roseggerstraße 12, A-8700 Leoben.

microscale compared to testing at the macroscale is the ability of probing the constituents of a complex microstructure with high spatial resolution using local micromechanical testing techniques [2]. As such, one can characterize the mechanical properties of i.e. individual grains, grain boundaries, phases and interfaces.

Besides the local plastic properties, fracture at the micrometer length scale has attracted severe attention during the last decade. For instance, Di Maio and Roberts first reported on microcantilever bending tests to evaluate the fracture toughness of thin coatings [6]. Furthermore, thin film intermetallic cantilevers were used to understand the fracture behavior of TiAl [7]. Later, micro bending was used to determine the toughness for brittle materials like oxides [8], amorphous carbon coatings [9], thin films [10,11], single crystalline silicon [4,12], metallic glass [13], quartz [14] and microporous silver [3].

Linear elastic brittle fracture occurred in all mentioned studies, i.e. the sample broke after linear elastic loading and without noticeable plastic deformation. The concepts of linear elastic fracture mechanics (LEFM) can – under certain conditions – be used to evaluate the sample size independent critical stress intensity factor. This critical stress intensity factor is called fracture toughness K_{IC} and a material parameter under plane strain conditions. The most stringent condition for LEFM is the absence of pronounced notch tip plasticity, which does depend on the material strength, toughness, and stress state (see Fig. 1). While the plane strain state suppresses plasticity in the sample center, the sample surface always exhibits a plane stress state which causes high shear stress and promotes plasticity. Consequently, the varying stress state along the crack front leads to an intrinsic critical stress intensity K_I variation, which strongly limits the comparison of the fracture toughness of semi-brittle materials at the microscale [15]. One can obtain a valid material fracture toughness K_{IC} only if the sample size is substantially larger than the plastic zone size. Fig. 1 presents an overview of various materials, their fracture toughness, yield strength and plastic zone size.

At the macroscale, the minimum sample dimensions for obtaining a valid K_{IC} are defined in the ASTM standards E399 (Eq. (1)) [24], with D_{LEFM} being the shortest dimension of sample thickness, crack length and ligament size (the sample height reduced by the notch depth as marked in Fig. 2). σ_y is the 0.2% yield strength.

$$D_{LEFM} = 2.5 \left(\frac{K_{IC}}{\sigma_Y} \right)^2 \tag{1}$$

The sample size independent fracture toughness cannot be obtained as soon as one sample dimension dissatisfies Eq. (1). Only for extremely
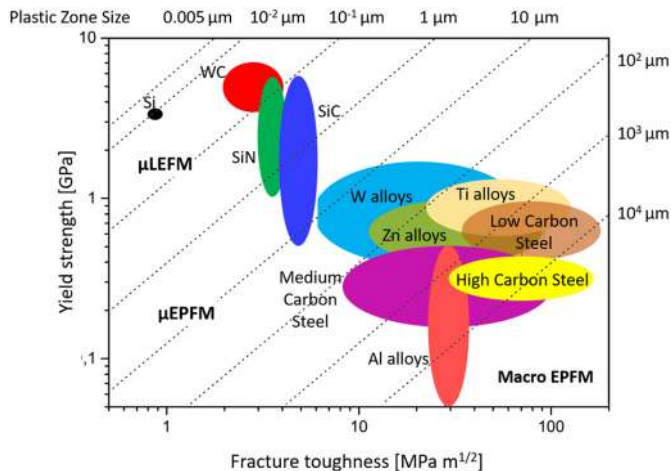

Fig. 1. Ashby map showing the plastic zone size of various materials depending on the fracture toughness and yield strength. Regions of linear elastic fracture mechanics at the microscale (µLEFM) and possible regions of elasto-plastic fracture mechanics at the microscale (µEPFM) are highlighted [4,16–23].

brittle materials (Fig. 1, upper left corner, area marked µLEFM) the plastic zone size is sufficiently small to measure a valid LEFM fracture toughness in micrometer sized samples.

In the last century, various approaches of elasto-plastic fracture mechanics (EPFM) had been developed to measure the fracture toughness of ductile materials using reasonable macroscopic sample sizes [25] (lower right corner in Fig. 1 denoted Macro EPFM). However, this establishment and standardization did not occur for microsamples. Only very brittle materials can be tested by linear elastic micro fracture mechanics (see Fig. 1) due to the stringent assumption of negligible plasticity around the notch tip. When using elasto-plastic fracture concepts, the critical dimension of the sample is D_{EPFM} (Eq. (2))

$$D_{EPFM} = 10...50 \frac{J_{Ic}}{\sigma_y}, \tag{2}$$

where J_{Ic} is the critical J integral under mode I loading. The pre-factor varies in literature from 10 [26] to 50 [27].

Wurster and co-workers [28] were the first to apply EPFM to micron sized samples and extended the microscale testing to other classes of materials, i.e. tungsten (see Fig. 1). Since their pioneering work, several authors have used EPFM to extend the number of material classes, which are tested at the microscale [20,29–32]. Various methods for sample preparation (e.g. micro electrical discharge machining [20] or femtosecond laser ablation [33]) and different cantilever geometries (rectangular, pentagonal [6,34] or triangular [14]) are used for small scale LEFM and EPFM today. The community discussed thoroughly the importance of FIB milled notches, which ideally are atomically sharp, free of residual stresses and without chemical ion interactions. Additionally, several different notch geometries are used: through thickness notch [11,29–31,35–38], bridge notch [4,32,39–42], chevron notch [14,20], and less prominent geometries. All of these notch geometries have specific benefits and are applied according to the specific project needs. Since standardized testing protocols do not exist, the comparison of the measured EPFM fracture toughness is challenging. In case of LEFM, the role of notch and sample geometry was investigated previously [4,42] and can be corrected – to some extend – by finite element modelling [15,42]. However, the influence of sample and notch geometries on the evaluated elasto-plastic fracture toughness for semi-brittle materials is not understood.

Moreover, significant differences exist among various research groups during data analysis and interpretation. In absence of an ASTM standard for micro fracture testing, Wurster and co-workers defined the conditional J-integral (J_Q) as the intersection of two fitted lines (crack blunting line and stable crack growth region) in the crack resistance curve (J vs. Δa curve, Δa is the crack extension) [28]. To determine J_Q, Bohnert et al. [20] – in contrast – use a blunting line parallel, which is shifted by a crack extension $\Delta a_t/2$. Here, a_t is the crack tip opening displacement with an opening angle of 90°. The third criteria for J_Q follows the spirit of the macroscale ASTM standard and allows for some variation in sample size. Pippan et al. [1] shift the blunting line by $\Delta a = 0.02W$ (W is the cantilever height) and define the intersection of this line with the J vs. Δa curve as J_Q. The forth approach to determine J_Q is based on a fixed crack extension $\Delta a = 0.2$ µm [35,37]. Hence, also data analysis and interpretation of J_Q lack appropriate standards. This shortcoming renders the quantitative comparison of toughness from different laboratories challenging.

The aim of this work is to shed light on the elasto-plastic fracture toughness for various notch geometries and methods for analyzing the crack length at the micron scale. We identify challenges during crack length measurements and discuss the important role of notch geometry and sample size in the regime denoted µEPFM in Fig. 1. Finally, some first guidelines are suggested for µEPFM testing.

i) Crack length measurement
a) Unloading stiffness method
b) *In situ* crack length

ii) Impact of notch geometry
c) Straight notch
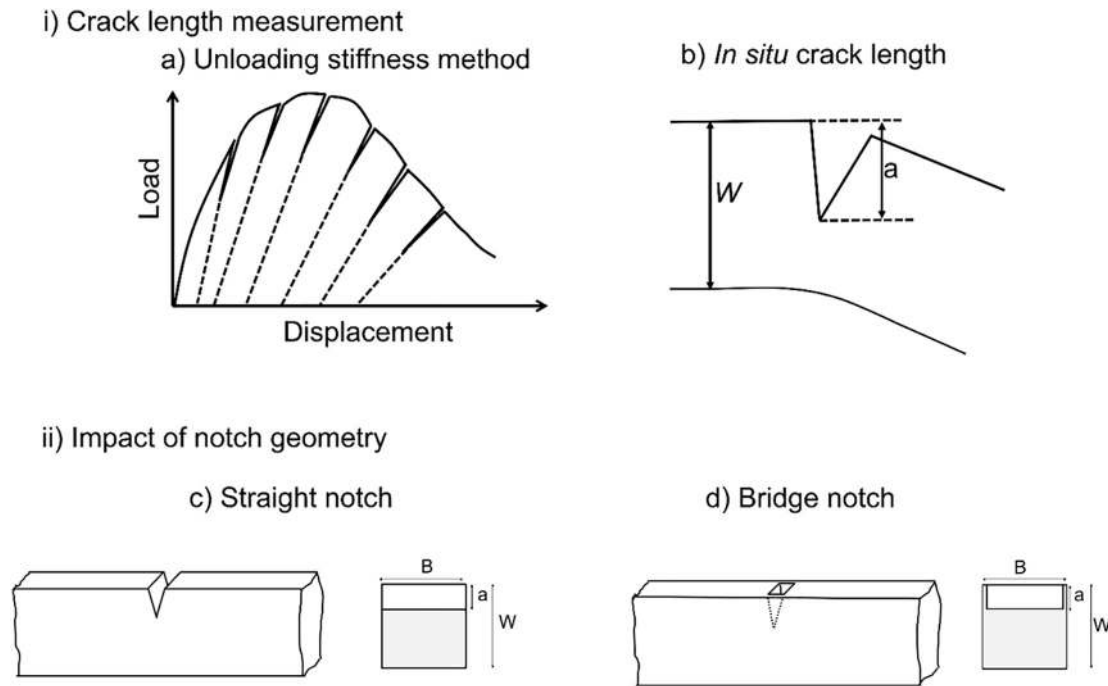### d) Bridge notch

Fig. 2. Schematic sketches of the crack length measurements using a) using the unloading stiffness or b) *in situ* SEM measurements. The different notch geometries are investigated: c) a straight through thickness notch vs. d) a bridge notch. Left images show an inclined side view while the right images display the fracture surface.

2. Experimental method

2.1. Material selection

In this study, we used a polycrystalline tungsten sheet (10 μm thick; supplied by GoodFellow GmbH, Hamburg, Germany) with submicron grains (~400 nm) for three reasons:

1. Tungsten is a model material exhibiting elastic isotropy and showing semi-brittle fracture at the micrometer length scale. Using Eq. (1) we estimate that the minimum sample size for obtaining K_{IC} is $D_{LEFM} = 100$ μm, which exceeds the metal sheet thickness. Hence, we expect an elasto-plastic fracture process. Assuming J_{Ic} of ≈ 1400 J/m^2 [22] and a yield strength of 3 GPa (obtained from tensile tests on wires with identical grain size), we expect a critical dimension for a valid J_{Ic} of $D_{EPFM} \approx 5\dots25$ μm according to Eq. (2).

2. Long range dislocation pile-ups near the neutral plane (or the tension/compression interface) are suppressed, because the grain size is considerably smaller than the cantilever dimensions. Hence, crack shielding – caused by dislocation pile-ups – does not change systematically during crack propagation because no long range back stresses occur.

3. The 10 μm thick sheet metal requires predominantly 2D FIB cutting which allows for an ample sample number due to the reduced milling time and, also, FIB redeposition is minimized.

2.2. Microsample preparation

All microcantilevers had a rectangular cross-section with the notch plane perpendicular to the rolling direction of the sheet metal and the crack propagation perpendicular to the normal direction of the sheet. The ratios height (W):width (B):length (L) of milled cantilevers were kept constant at 1:1:7. The cantilever height was maintained constant (6.5 to 7 μm). Each cantilever was prepared in three steps: i) plasma FIB assisted coarse cutting, ii) Ga FIB based medium and fine milling, followed by iii) notching and post-notch cleaning (in case of straight through thickness notches). The coarse cutting was performed by Xe plasma FIB milling (FEI Helios PFIB) using 30 kV energy and a current of 1.3 μA. The intermediate and fine milling as well as the notching

were made inside a Zeiss Auriga® dual beam microscope operated at 30 kV and equipped with a Nano Patterning and Visualization Engine (NPVE). The intermediate milling was carried out at 16 nA current until a dose of 40 nC/μm^2 was reached (16 nA||40 nC/μm^2) which is further reduced to 600pA||30 nC/μm^2 for fine milling.

The microcantilever beams were prepared with two notch types, through thickness and bridge notches. Three different notch-to-thickness (a_0/W) ratios 0.2, 0.3 and 0.4 were prepared for each notch type. In order to achieve a sharp notch tip, 30 kV and 10 pA were selected for notching. The doses for the various depths were optimized by inspecting cross-sections on the same tungsten sample (see appendix of [39]). Depending on the target a_0/W, we used doses of 80 nC/μm^2, 160 nC/μm^2, 260 nC/μm^2. For cantilevers with through thickness notches, the side surfaces were re-polished to assure a uniform depth throughout the sample width and to avoid side-notch effects (over-FIBing). The initial notch depth (a_0) was measured by SEM imaging before and/or after the micro fracture experiments. In case of cantilevers with bridge notches, we kept the bridges thin and symmetric. Redeposition on the cantilever surface was reduced by a successive reduction of milling current and by using a thin sheet metal instead of bulk tungsten.

2.3. Microcantilever fracture experiments

The *in situ* micro fracture experiments were performed in a Zeiss Gemini 500 SEM. An ASMEC UNAT II indenter equipped with a 10 μm wide diamond wedge was used for cantilever bending in a displacement open loop mode. The crack initiation and propagation was observed and recorded with high resolution *in situ* imaging during the entire micro bending test. In few cases, undesired slip of the wedge indenter on the sample surface was observed. However, this slip only occurred near the end of the experiment and such experiments were not used in the analysis. Moreover, a precise alignment of the wedge indenter is vital for reliable experiments, because such alignment assures that the wedge indenter forms a line contact and avoids any torque. We aligned the sample on the macroscale similar to the protocol introduced in the appendix of [43] and we did not rely on microscopic alignment inside the SEM.

One main challenge in elasto-plastic fracture testing at the micro-scale is to accurately measure the crack length throughout the experiment. In this study, two techniques are used for crack length measurements: (i) The crack length was measured indirectly using the unloading stiffness of the cantilever [28,35,43,44] (see also Section 2.4). (ii) The crack length at the surface is directly observed based on *in situ* SEM imaging [28,29,31,36]. In this case, we define the crack length as the vertical distance from the top-surface of the cantilever stub to the visible crack tip (as schematically shown in Fig. 2b). Note that the measurements are corrected for the sample tilt and these measurements are only possible for through thickness notches.

The validity of the crack length measurements was analyzed by post-mortem cross-sectioning on three microcantilevers. In addition, we observed the crack length variation along the crack front.

2.4. Fracture toughness analysis

The fracture toughness of tungsten is estimated by the *J*-integral approach, which was implemented in earlier elasto-plastic micro fracture experiments [28]. The *J* integral for elasto-plastic materials is obtained by adding the elastic and plastic contributions according to Eq. (3).

$$J^{(i)} = J^{(i)}_{elastic} + J^{(i)}_{plastic} \qquad (3)$$

The elastic contribution $J_{elastic}$ is obtained from LEFM, where $K^{(i)}_{IQ}$ represents the plane strain stress intensity factor at time increment i (calculated from Eqs. (4) and (5)).

$$J^{(i)}_{elastic} = \left(K^{(i)}_{IQ}\right)^2 \frac{(1-\nu^2)}{E}, \qquad (4)$$

$$K^{(i)}_{IQ} = \frac{F^{(i)}_Q L}{BW^{3/2}} f\left(\frac{a^{(i)}}{w}\right), \qquad (5)$$

Here, ν is the Poisson's ratio, E is the elastic modulus of the material, $F^{(i)}_Q$ is the force at time increment i and L is the bending length from the notch to the point of force application. All other cantilever dimensions are defined in Fig. 2. The dimensionless factor $f(\frac{a}{W})$ for rectangular cantilevers (Eq. (6)) is taken from Matoy et al. [8] and a through thickness notch is assumed in all samples.

$$f\left(\frac{a}{w}\right) = 1.46 + 24.36\left(\frac{a}{W}\right) - 47.21\left(\frac{a}{w}\right)^2 + 75.18\left(\frac{a}{w}\right)^3. \qquad (6)$$

The unloading stiffness (k) is one way of determining the crack length in this study. This stiffness was calculated at several unloading cycles and used to estimate the ligament length ($W - a_i$) using (Eq. (7))

$$W - a_i = \sqrt[3]{\frac{4kL^3}{BE}}. \qquad (7)$$

The ligament length is used to obtain the crack length (a_i) at time increment i. Due to the use of a wedge indenter, no residual imprint was observed which eliminates the requirement of force-displacement data correction.

The plastic contribution to the *J* integral ($J_{plastic}$) is calculated according to Eq. (8),

$$J^{(i)}_{plastic} = \int \frac{\eta A_{Plasticlocal}}{B(W-a_i)}, \qquad (8)$$

where η is a constant ($\eta = 2$). $A_{Plasticlocal}$ is the plastic work during crack propagation. We assume that plasticity is confined within the plastic zone at the crack tip and therefore obtain the plastic work by measuring
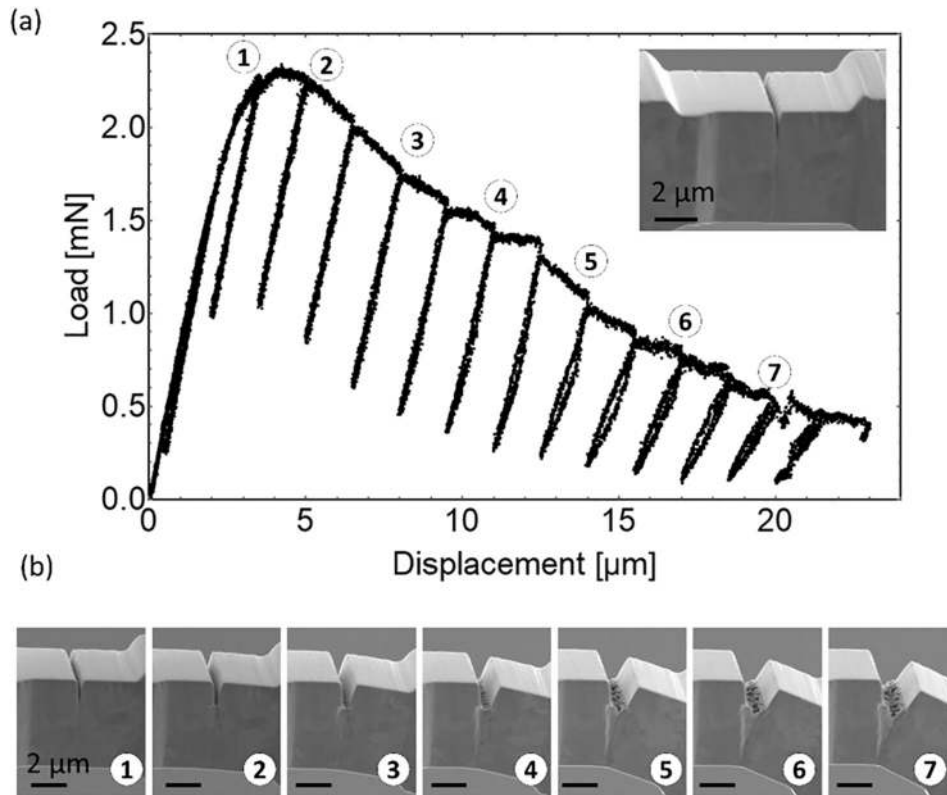

Fig. 3. a) Representative load vs. displacement curve for tungsten cantilevers with a straight through thickness notch. The inset represents an SEM image of the initial notch. b) *In situ* SEM snapshots of the crack extension at locations indicated in (a).

the area under the load-displacement curve. Finally, the complete J integral at each instant of time (i) is calculated (Eq. (9)).

$$J^{(i)} = \left(K_{IQ}^{(i)}\right)^2 \frac{(1-\nu^2)}{E} + \frac{2 * A_{Pl(i)}}{B * (w-a_0)} \qquad (9)$$

In absence of ASTM standards, the conditional J integral (J_Q) is obtained from Pippan's transfer of ASTM standards for small scale experiments [1,38]. We fitted a polynomial function to the analyzed crack resistance curve (J vs. Δa) and use the blunting line offset of $\Delta a = 0.02\ W$ to determine J_Q [38]. Finally, we calculate K_{IQ} from J_{IQ} as given in Eq. (10) for a quantitative comparison of the fracture toughness.

$$K_{IQ} = \sqrt{J_{IQ} \frac{E}{(1-\nu^2)}} \qquad (10)$$

3. Results

3.1. Fracture experiments on samples with through thickness notches

The representative load-displacement curve with multiple partial unloading segments shows the elasto-plastic fracture in ultra-fine grained tungsten sheets (Fig. 3a). The partial unloading segments, which are required to calculate the crack propagation, are seen throughout the deformation. After initially showing elastic behavior, the load vs. displacement curve documents significant plasticity after a few initial unloading cycles (from point 1 onwards in Fig. 3a). The pronounced plasticity in the vicinity of the notch tip is also documented by the snapshots in Fig. 3b.

Besides using the unloading stiffness to calculate the crack extension, we directly measured the crack length on the surface using SEM snapshots that were recorded at a frame rate of 1 s^{-1}. The first significant crack extension is accompanied by plasticity and appears at location (2) in Fig. 3a and b. The crack grows along the intended plane
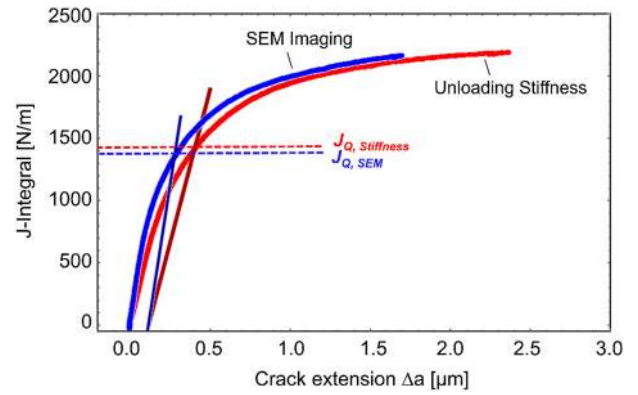

Fig. 5. Crack resistance curve of the sample presented in Fig. 3 (through thickness notch, $a/W = 0.24$). The red data is obtained from the unloading stiffness and the blue data is obtained by *in situ* SEM imaging of the advancing crack. (For interpretation of the references to color in this figure legend, the reader is referred to the web version of this article.)

while the plastic zone size significantly increases. On the fracture surface, evenly distributed dimples are identified (see (6) and (7) of Fig. 3b).

The detailed analysis of the microcantilever fracture data is shown in Fig. 4. The stiffness, which is obtained from the unloading segment slope, continuously reduces and documents stable crack growth in tungsten cantilevers (see Fig. 4b). The individual measurements (dots) are subsequently described by a second order polynomial fit. Subsequently, this cantilever stiffness is used to calculate the crack extension according to Eq. (7) (see black points and black line in Fig. 4c). The crack length obtained from *in situ* SEM snapshots is plotted as blue triangles with a fitting curve. At the beginning of the experiment, both methods show a similar crack length; however, the crack length obtained from *in situ* SEM snapshots is smaller compared to the crack length obtained
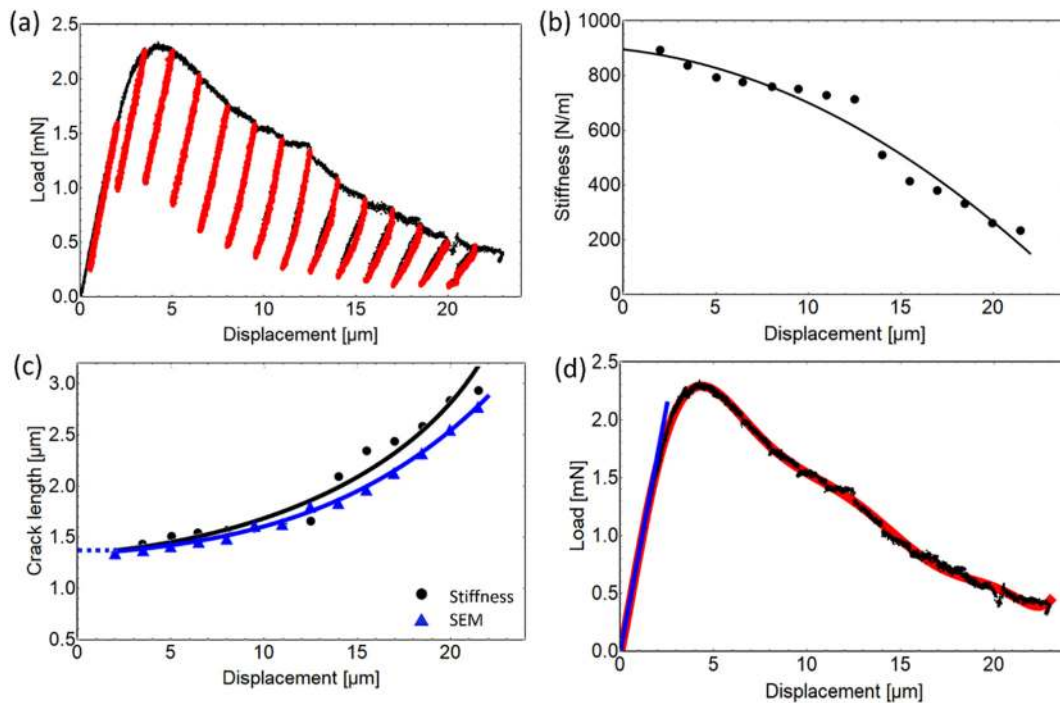

Fig. 4. Analysis of the load vs. displacement curve presented in Fig. 3a. a) Raw load vs. displacement data with unloading segments fitted for analyzing the unloading stiffness. b) Change in unloading stiffness due to crack extension. The line shows a polynomial fit to the data. c) Crack length vs. indenter displacement derived from the unloading stiffness and *in situ* SEM imaging. d) Polynomial fit to the load vs. displacement curve to calculate the total absorbed energy.
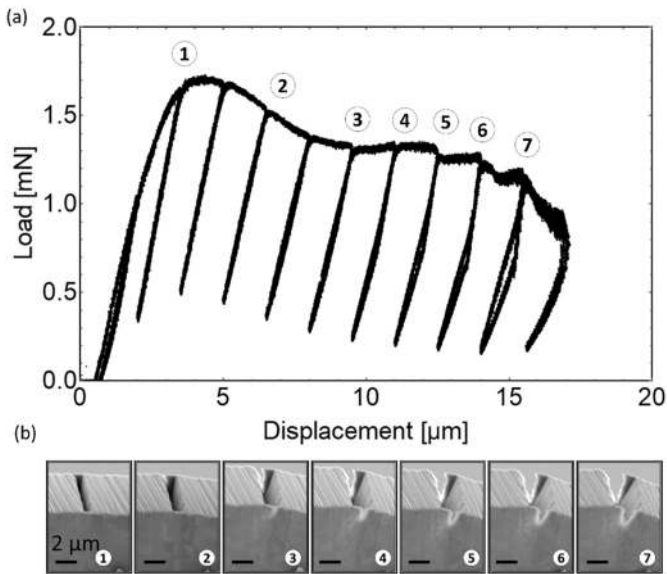
Fig. 6. a) Representative load vs. displacement curve for tungsten cantilevers with a bridge notch. b) *In situ* SEM snapshots of the crack extension at locations indicated in (a).

from unloading stiffness during the later stage of the experiment. The origin of this behavior is discussed in Sections 3.3 and 4.1.

Finally, the load displacement curve (red curve in Fig. 4d) is described by a polynomial equation that is chosen to ease the numerical integration of the absorbed plastic energy ($A_{Pl(i)}$) during the cantilever bending experiment.

The elasto-plastic J integral for through thickness notch cantilevers is quantified by addition of the elastic ($J_{elastic}$) and plastic ($J_{plastic}$) contribution as given in Eq. (9). The fracture behavior is analyzed by inspecting the crack resistance curve (J vs. Δa) obtained from both crack length evaluation techniques (see Fig. 5). Both techniques suggest a similar fracture behavior and both techniques give a similar critical J-Integral. If one compares the conditional J-integral (J_Q) by Pippan's ASTM transfer

criterion [1], only small differences of $J_{Q,Stiffness}$ and $J_{Q, SEM}$ within the error bars are seen. In all samples, the unloading stiffness method results in larger crack extensions and the corresponding crack resistance curves is stretched horizontally. We will discuss the origin of this behavior in Sections 3.3 and 4.1.

In total, we have tested successfully 12 cantilevers with through thickness notches and these cantilevers follow the same fracture behavior as shown here. The combined data will be presented in Chapter 4.

3.2. Fracture experiments on samples with bridge notches

The cantilevers with a bridge notch show characteristic similarities and differences to the ones with through thickness notches, as seen by the representative load-displacement curve in Fig. 6a. Similar to the through thickness notches, the bridge notch cantilevers shows an elasto-plastic fracture process. However, the load remains constant at 1.3 mN and does not continuously reduce as for through-thickness notches. Also the *in situ* SEM information is different: a measurement of the crack extension by SEM remains impossible here although it was possible for through thickness notches. Moreover, the progressive crack opening at the bridge (see Fig. 6b) cannot be used to measure the crack length. Hence, the fracture analysis is limited to the unloading stiffness method for bridge notch cantilevers.

A detailed analysis of a bridge notch cantilever is shown in Fig. 7. The representative load vs. displacement curve shows pronounced plasticity starting at the 2nd unloading cycle, i.e. at a total indenter displacement of 3 μm. The stiffness of each consecutive unloading segment drops during deformation (see Fig. 7b) which is used to calculate the crack length at certain indenter displacements (Fig. 7c). The initial notch depth is obtained from post-mortem SEM imaging for all bridge notch cantilevers, as shown in inset of Fig. 7c. The initial notch depth measured via the SEM (blue line in Fig. 7c) is ≈1.7 μm for the present cantilever. This measurement matches well with the crack length determined from the unloading stiffness (black data).

In total, we have successfully tested 10 cantilevers with bridge notches and applied the unloading stiffness method. The combined data will be presented in chapter 4.
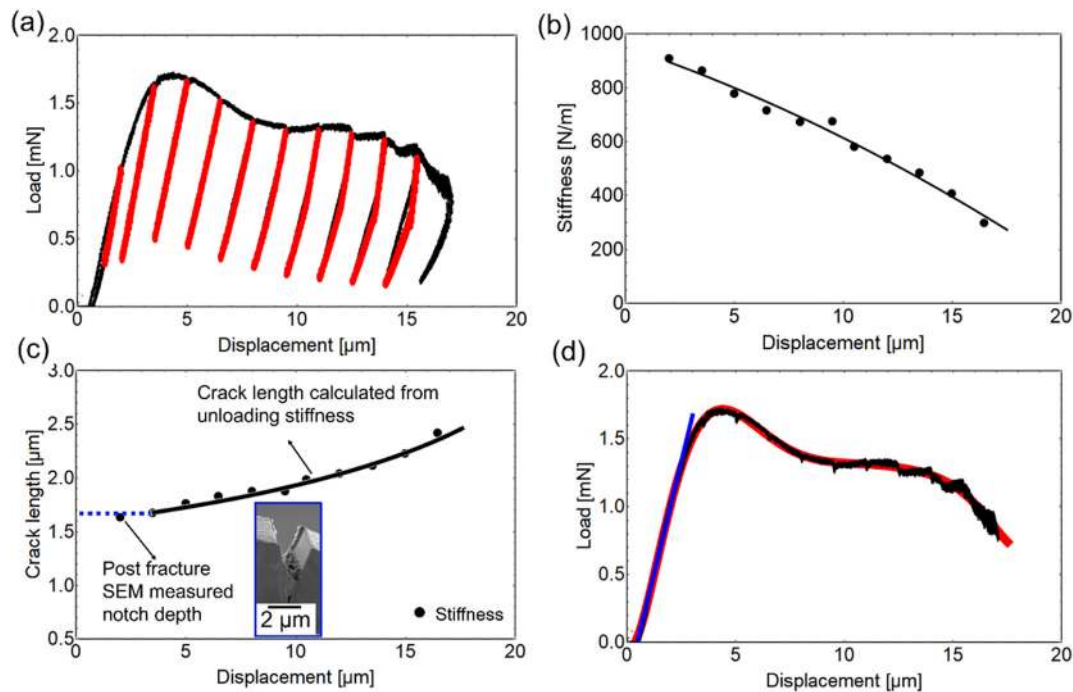

Fig. 7. Analysis of the load vs. displacement curve presented in Fig. 6a for a bridge notch cantilever. a) Raw load vs. displacement data with unloading segments fitted for analyzing the unloading stiffness. b) Change in unloading stiffness due to crack extension. c) Crack extension vs. indenter displacement derived from the unloading stiffness. d) Polynomial fit to the load vs. displacement curve to calculate the plastic energy.
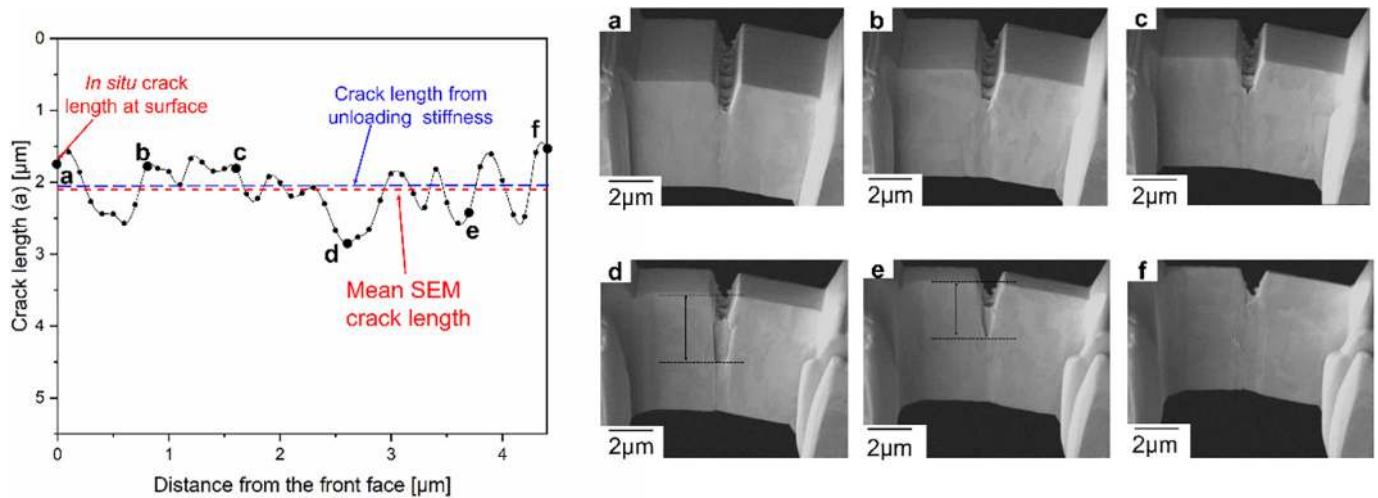
Fig. 8. Through thickness measurements of the crack length at a crack extension close to $\Delta a_{critical}$, i.e. at the corresponding crack extension to J_Q. The individual cross-sections are indicated in the plot. For selected examples the measured crack length is indicated in black.

3.3. The homogeneity of the crack length

The discrepancy of the crack length measurements by the stiffness method and by *in situ* SEM imaging raises questions about the shape of the crack front. For this purpose, we performed serial sectioning of the crack front at (i) a critical crack extension $\Delta a_{critical}$ (Fig. 8) as well as (ii) the maximum displacement of ≈15 μm (Fig. 9). The initial crack was a through thickness notch with an a/W ratio of 0.2 in both cantilevers.

Overall, the crack is straight, symmetric and without crack tunneling in the cantilever center. However, the crack shows pronounced length variations with local crack advancements (see Fig. 8d or Fig. 9e). At the critical crack length $\Delta a_{critical}$, the ratio of the longest crack segment (≈3 μm) and the shortest crack segment (≈1.5 μm) is 2 and the crack remained at its initial position in one location while it grew to twice its length at another (see Fig. 8). The absolute differences of the crack length are more pronounced for longer cracks (the minimum and maximum crack length is ≈2.7 μm and ≈5 μm in Fig. 9). This observation documents the challenges in determining the crack length and the toughness– in samples in which the microstructural length and the radius of the fracture process zone are similar to the sample size.

4. Discussion

4.1. Comparison of crack length determination methods

We have obtained the crack length by the unloading stiffness method and from snapshots recorded during *in situ* SEM imaging. While the unloading stiffness method gives the average crack length, SEM imaging only provides the crack extension at the surface. Hence, the SEM based method is blind to the crack length variation along the crack front and the obtained crack length might differ from the unloading stiffness method. One example for pronounced differences between the methods is Fig. 5, in which the maximum crack extension is considerably different for the unloading stiffness method compared to the method that uses SEM imaging. Moreover, the data presented in Figs. 8 and 9 shows the crack length heterogeneity during crack growth and the shorter crack length on the surface.

Please note that the pronounced crack length variation across the sample (Figs. 8 and 9) is not caused by experimental artefacts. This variation is caused by the microstructure variation in the fracture process zone. The local grain orientation causes a strong variation in the local
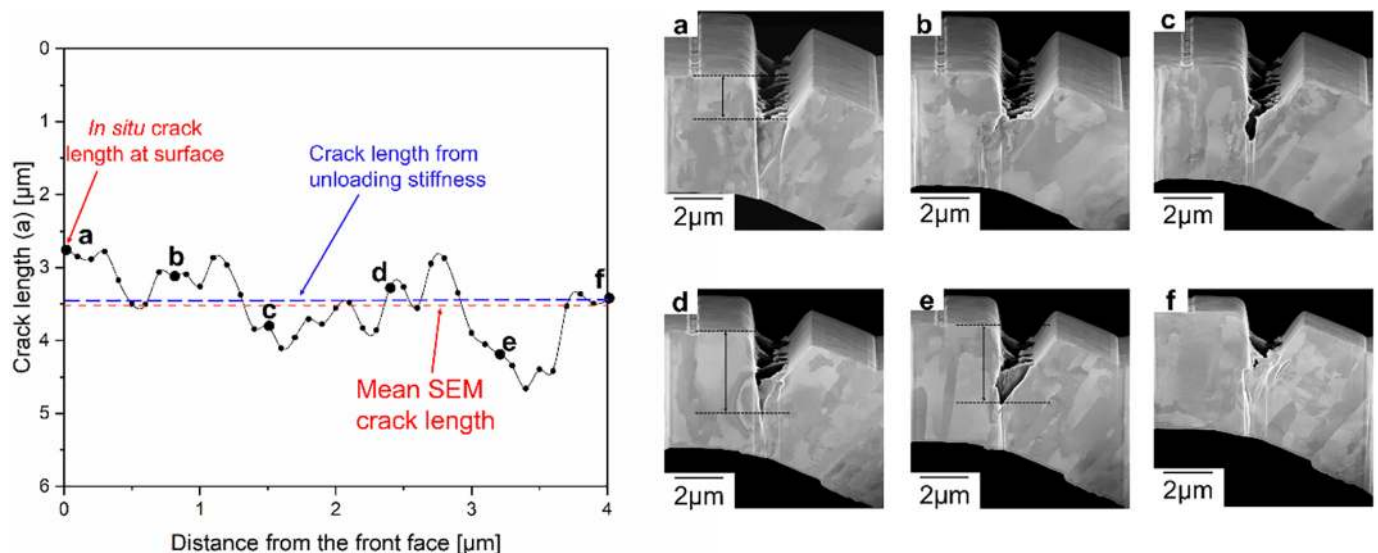

Fig. 9. Through thickness measurements of the crack length at the maximum displacement. The individual cross-sections are indicated in the plot.

crack growth resistance, e.g. differently oriented cleavage planes and crack shielding by dislocation pile-ups at grain boundaries. While the crack length variation documents the strength of micro fracture testing in quantifying fracture mechanisms, the variation also emphasizes the difficulties of determining meaningful material parameters at small length scales. At these scales, the local crack length variation is significant with respect to the crack length (e.g. the crack length doubled in Fig. 8).

It should be noted that the critical J_{IQ} is not altered significantly by neither the crack length differences due to the two methods nor the crack length variation (see Fig. 5). Moreover, crack branching and deflection is observed, if we employ an alternate cantilever geometry with crack growth in the sheet rolling direction. Since crack branching in complex geometries - like the present cantilever geometry – cannot be captured by analytical models, we do not address this geometry here.

Even when investigating all cantilevers, the identified J_{IQ} does not vary significantly from the unloading stiffness method compared to the method based on in situ SEM imaging. By comparing 17 cantilevers with varying a/W ratio, we observe that the fracture toughness is 5% smaller if obtained by in situ SEM imaging than if obtained by the unloading stiffness (see Figs. 10, 5% difference is calculated from the average toughness values irrespective of initial notch depth). The small differences could be explained by a curved crack front advancing further in the sample center compared to the sample surface. However, as documented in Figs. 8 and 9 this was not observed. Hence, the origin of the apparently smaller toughness analyzed by in situ SEM imaging remains unclear. Please note that the toughness was obtained on the same cantilever by both methods.

4.2. Effect of notch geometry

Secondly, we analyze the importance of the notch geometry (straight through thickness vs. bridge notches) on the obtained fracture toughness. The geometry factor $f(\frac{a}{W})$ differs for through thickness and bridge notches according to LEFM [42]. In LEFM cantilevers with bridge notches, crack initiation is ideally localized and sequential, i.e. the crack initiates first in the bridges and after bridge failure the main crack develops in the center of the notch. In contrast, during elasto-plastic fracture much larger crack and plastic process zones develop which do not allow to spatially or sequentially separate failure sites. Moreover, the plasticity leads to large deformations which are less defined than during LEFM and which influence the crack driving force. The uncertainty of the
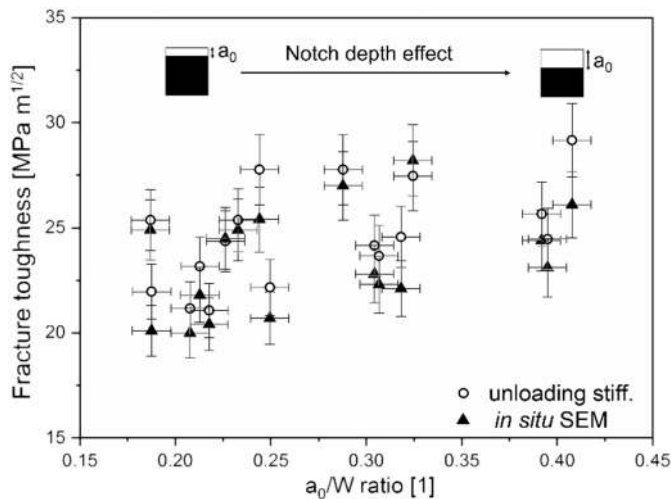
crack shape during the fracture process prevents a proper implementation of the evolving notch geometry, i.e. the elastic contributions to the J integral have a high uncertainty. Moreover, the thin bridges are entirely in plane stress state while the main crack is assumed to fail predominantly under plane strain. Please note that the plane stress state leads to a larger plastic zone according to fracture mechanics. This enlarged plastic zone is observed in this study in the present bridges (see Fig. 6b (3–5)). Due to all these reasons, it is expected that the obtained fracture toughness shows pronounced differences for bridge notch and through thickness notch cantilevers in semi-brittle materials.

The differences of bridge notch cantilevers and through thickness notch cantilevers is quantified in Fig. 11. Since the crack tip is invisible for bridge notches, we only use crack lengths that were obtained from the unloading stiffness method for this comparison. The results show that bridge notch cantilevers appear to have a higher fracture toughness than through thickness notch cantilevers for all a/W ratios. The toughness obtained from bridge notch cantilevers is up to 20% higher than the one from through thickness notch cantilevers. This difference is of the same order as the differences in geometry factor for the two notch types according to LEFM [42]. One could hypothesize that the difference in the present EPFM study originates from an unknown geometry factor. However, since the J-Integral is dominated by the plastic contribution, the changes in the LEFM based contribution do not significantly alter the total J-Integral. More likely, the differences originate from the pronounced plasticity in the bridge notches.

In summary, the obtained fracture toughness strongly depends on the chosen notch geometry. Due to the unknown geometry for the bridge notches evolving during the fracture process, due to the non-localized and non-sequential fracture with large process zones and due the plasticity caused by the plane stress state in the material bridges, it is highly recommended to use through thickness notches for semi-brittle materials. Since bridge-notches appear inferior compared to straight notches for EPFM, we measured the crack front shape for the superior geometry (Fig. 9) but not for the inferior cantilever geometry.

4.3. Effect of notch depth (a_0/W)

Geometrical constraints exist for the cantilever to determine a size independent J_{IC}. The dominant constraint is the minimal sample dimension, which is estimated from Eq. (2). For ultrafine grained tungsten with $J_{IQ} = 1400$ N/m and $\sigma_y = 3$ GPa, we estimate the minimum cantilever dimension ranging from 5 to 25 μm. In this study, the cantilever width and height was 8 μm and the ligament size

Fig. 10. Fracture toughness (K_{IQ}) of through thickness microcantilever as function of notch depth (a_0/W), calculated by two crack length methods; a) unloading stiffness (circles) and b) in situ SEM imaging (triangles).
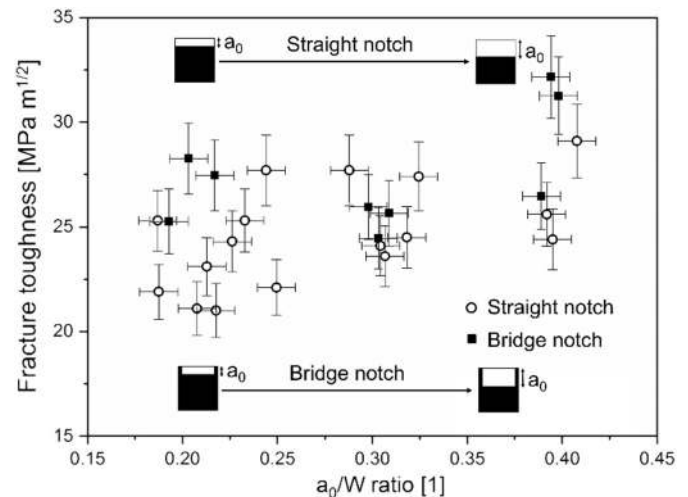

Fig. 11. Fracture toughness (K_{IQ}) of ultrafine grained tungsten as a function of notch geometry (through thickness vs bridge) and notch depth (a_0/W).

$(W - a_0)$ is 5 μm at $(a_0/W) = 0.4$. All of these dimensions are at the lower limit of the required size according to Eq. (2). To investigate the influence of the shortest dimension, i.e. ligament size, we vary it and draw conclusions about the minimum cantilever dimension to obtain size independent J_{IQ}.

Figs. 10 and 11 suggest that the extracted fracture toughness is size dependent: larger a_0/W ratios, i.e. smaller ligament sizes, lead to higher apparent K_{IQ}. While a mild change is observed for K_{IQ} (Figs. 10 and 11), the crack resistance curves document the vastly different fracture behavior, as shown in Fig. 12. The large changes in the crack resistance curve must not be interpreted as size scaling of the fracture toughness, because the microstructural dimensions are identical irrespective of the initial crack length. Hence, intrinsic scaling of the fracture toughness originating from the material is excluded. Note that Fig. 12 shows the crack resistance curve: above a threshold critical crack length, the J-value increases significantly and then the gradient of the J-value decrease as the crack progresses. This behavior is typical for crack resistance curves even at the macroscale. In this diagram, we added J_{IQ} for the individual samples according to Pippan's transfer criterion. We observe that the extracted toughness increases with decreasing ligament size (increasing a_0/W ratio).

Based on LEFM, one could hypothesize that a steady state behavior is reached above a critical length and that the fracture behavior becomes dimension independent above this crack length. This hypothesis is not the case. Longer initial notches (smaller ligament sizes) show a significantly tougher crack-growth (see Fig. 12). The ligament dependent fracture toughness was found at the macroscale showing a mild change in initiation toughness but tremendous differences in the crack resistance curve [27,45]. Generally at the macroscale, longer ligaments resulted in tougher crack resistance curves because the plastic zone is not constrained [27,45]. However, very short ligaments result in an increased crack resistance curve at the macroscale [27]. The same toughness increase with decreasing ligament size is observed at the microscale in this study. The stress state and plastic zone size differ significantly for short and long initial ligaments and the behavior of the tungsten cantilevers is not dominated by elasticity, especially for deep initial notches. Consequently, we cannot report size independent fracture toughness or crack resistance curves (see Fig. 12) within this study. Hence, the elastic-plastic fracture toughness depends on a crack length and geometry for micrometer components, e.g. MEMS.

We conclude that a conservative estimate of the pre-factor is required in Eq. (2) for a size independent crack resistance curve. The factor should – in accordance with the macroscale and ASME standard – be 50 [27] and not 10 (as used in the present study).
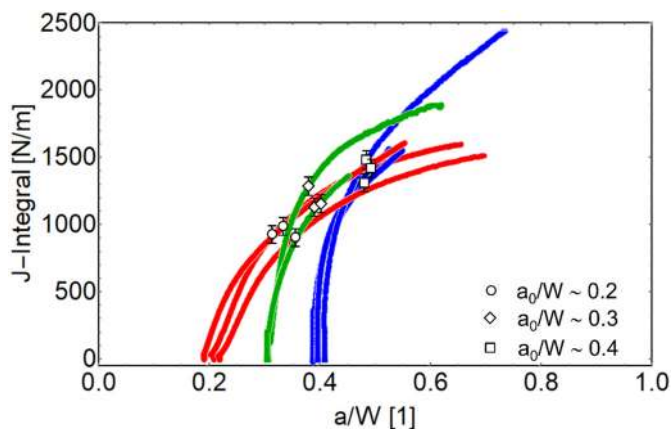

Fig. 12. The crack resistance curve for several cantilevers with through thickness notches calculated from *in situ* SEM crack measurement. Each point superimposed to the individual crack resistance curve indicates the J_{IQ} value according to Pippan's transfer criterion.

5. Recommendations for EPFM

Based on this study of elasto-plastic fracture mechanics, we recommend the subsequent workflow for analyzing the fracture toughness at the microscale. To execute this workflow, an a priori estimate of the strength and toughness is beneficial.

I) Identify if LEFM is applicable. If possible, choose a sample size which allows one to observe brittle fracture (Eq. (1)). In this case, we recommend to use samples with these dimensions because all challenges (determine crack length and shape, the criterion for crack initiation and growth) are prevented.
   In cases, in which EPFM cannot be excluded safely, we recommend a microcantilever with straight through thickness notch, as this shape is also applicable in EPFM.

II) Sample requirements for EPFM. If the material and experimental constrain do not allow for LEFM compatible samples, the best approach is to use EPFM according to the present approach [1,28,29].
   a. However, stringent assumptions for a minimum sample size exist. Eq. (2) defines the minimum sample dimensions and it is recommended to use a conservative pre-factor significantly higher than 10.
   b. If one wants to determine a sample size independent fracture toughness, we recommend that the fracture process zone should be substantially smaller than the sample size. This requirement might be challenging for single crystals, in which dislocations move to large distances.

III) Prepare the sample using FIB. Through thickness notches and a a/W ratio of 0.2–0.3 are recommended for EPFM. These parameters result in an elbowed fracture resistance curve as prescribed by macroscale standards.
   The cantilevers should be at least 5 times longer than their width and heights in order to limit the influence of shear stresses [42]. While bridge notches are beneficial in brittle materials, it is not recommended to use bridge notches for EPFM as they overestimate the toughness (see Fig. 11). We also recommend to use rectangular beam cross-sections as plasticity in the compression domain cannot be excluded for pentagonal beams.

IV) Avoid residual imprints. Raw force-displacement data is well-suited for measuring the crack propagation by the unloading stiffness method. However, a residual imprint alters the displacement data, which must be corrected before calculating the crack length [29]. It is recommended to use a wedge indenter with a line contact and a minimum cantilever length of 5 times the sample height W. These precautions prevent a residual imprint, as in the present study. Note that the wedge indenter requires alignment in two directions because – otherwise – unwanted torque is introduced.

V) Use an intrinsically displacement controlled device. The testing rig has to follow a load-displacement curve of the sample including a load decrease for large displacement of through thickness notches. Hence, an intrinsically displacement controlled device is required. Force controlled or pseudo displacement controlled indenters might not be able to follow the force displacement curve.

VI) Determine the crack length *in situ*. The unloading stiffness method probes a mean crack length which is different than the surface crack length obtained by *in situ* SEM imaging. This study shows that the crack length depends on the microstructure and the toughening mechanism in the process zone at this length scale. Both measurements individually cannot reflect the crack length distribution. Both measures give a more complete understanding of the fracture mechanisms.
   In passing, both methods result in a similar crack initiation

toughness with slightly higher values for the unloading stiffness method. Hence, the initiation toughness from *in situ* SEM imaging is more conservative.

VII) Is the crack front straight? It is recommended to perform serial sectioning on the crack to investigate the homogeneity of the crack extension. In case of large variations in the crack length, the extracted *J* is an average of different toughening mechanisms in the crack process zone. When a microstructure independent toughness is required, crack length variations cannot be accepted and larger sample sizes are required, that representatively average the microstructure.

VIII) How to determine the crack initiation toughness? Several criteria for the crack initiation toughness had been proposed. We recommend to use Pippan's ASTM transfer [1] that includes size scaling. We note that when fitting the steady state crack extension by a polynomial function eases the application of Pippan's transfer criterion. Also, note that we strictly follow the suggestion of Pippan with $\Delta a = 0.02W$. Using different Δa values can result in substantially different toughness values.

IX) Is $J_{IQ} = J_{IC}$? A critical assessment is required after EPFM analysis to determine the validity of the extracted fracture toughness K_{IQ} or J_{IQ}. One needs to show that J_{IQ} (or K_{IQ}) is size independent. We recommend to

   a. Use Eq. (2) to evaluate, if the sample size was large enough.

   b. Test at least two different sample sizes (width, height, crack length or ligament size) and proof the size independence of the crack resistance curve.

   c. Show the crack resistance curves for all samples and show that these curves have a similar shape, preferably with a pronounced elbow.

Otherwise, a system (i.e. material plus geometry) dependent fracture behavior is measured and not a size independent material property.

6. Conclusions

Linear elastic fracture mechanic (LEFM) experiments are commonly used for measuring material properties at the microscale and during the development of hard coatings. However, this approach for extracting valid fracture toughness is only applicable to very brittle materials. To extend the applicability of small scale testing to elasto-plastic fracture mechanics (EPFM), the present study present a critical evaluation of its current state. To improve the understanding of fracture mechanics, the reliability and generality of the apparent fracture toughness, within this work we assessed different sample geometries and different methods for determining the crack length. We can conclude:

I) The obtained fracture toughness depends on the method used for determining the crack length. The unloading stiffness shows a mildly larger toughness compared to *in situ* SEM imaging. Hence, the SEM approach results in a more conservative fracture toughness.

II) The crack length is subjected to significant variations across the crack width. The local crack length depends on toughening mechanisms in the local crack process zone. If the process zone size is similar to the sample size, a size and microstructure dependent fracture toughness is obtained.

III) The extracted toughness depends on the geometry of the initial notch. The bridge notches – which can be beneficial in LEFM – show extended ductile tearing and an elevated fracture toughness. Therefore, only through thickness notches are recommended for EPFM.

IV) It is vital to confirm the size independence of the initiation

toughness and the crack resistance curve by using Eq. (2), by presenting the crack resistance curves and by validating the geometry independence of the crack resistance curve.

V) To assure a comparability of the EPFM fracture toughness at the microscale, the community needs to develop standardized testing protocols and similar geometries. The workflow presented in this study is only the first step.

VI) Challenges arising from sample size scaling remain and need to be addressed in the future especially when the plastic and fracture process zones reach the sample dimensions.

Data availability statement

The raw/processed data required to reproduce these findings can be shared on request.

Credit authorship contribution statement

Ashish Kumar Saxena: Investigation, Formal analysis, Writing - original draft, Writing - review & editing. **Steffen Brinckmann:** Conceptualization, Methodology. **Bernhard Völker:** Conceptualization, Formal analysis. **Gerhard Dehm:** Writing - review & editing, Supervision. **Christoph Kirchlechner:** Conceptualization, Methodology, Writing - original draft, Writing - review & editing, Supervision.

Declaration of competing interest

We hereby confirm that none of the authors has any interests besides pushing science. Hence: none.

References

[1] R. Pippan, S. Wurster, D. Kiener, Fracture mechanics of micro samples: fundamental considerations, Mater. Des. 159 (2018) 252–267, https://doi.org/10.1016/j.matdes.2018.09.004.

[2] G. Dehm, B.N. Jaya, R. Raghavan, C. Kirchlechner, Overview on micro- and nanomechanical testing: new insights in interface plasticity and fracture at small length scales, Acta Mater. 142 (2017) 248–282, https://doi.org/10.1016/j.actamat.2017.06.019.

[3] C. Chen, S. Nagao, K. Suganuma, J. Jiu, T. Sugahara, H. Zhang, T. Iwashige, K. Sugiura, K. Tsuruta, Macroscale and microscale fracture toughness of microporous sintered Ag for applications in power electronic devices, Acta Mater. 129 (2017) 41–51, https://doi.org/10.1016/j.actamat.2017.02.065.

[4] B.N. Jaya, C. Kirchlechner, G. Dehm, Can microscale fracture tests provide reliable fracture toughness values? A case study in silicon, J. Mater. Res. 30 (2015) 686–698, https://doi.org/10.1557/jmr.2015.2.

[5] W.C. Oliver, G.M. Pharr, An improved technique for determining hardness and elastic modulus using load and displacement sensing indentation experiments W, J. Mater. Res. 7 (1992) 1564–1583, https://doi.org/10.1080/14786435.2012.658449.

[6] D. Di Maio, S.G. Roberts, Measuring fracture toughness of coatings using focused-ion-beam-machined microbeams, J. Mater. Res. 20 (2005) 299–302, https://doi.org/10.1557/JMR.2005.0048.

[7] T.P. Halford, K. Takashima, Y. Higo, P. Bowen, Fracture tests of microsized TiAl specimens, Fatigue Fract. Eng. Mater. Struct. 28 (2005) 695–701, https://doi.org/10.1111/j.1460-2695.2005.00893.x.

[8] K. Matoy, H. Schönherr, T. Detzel, T. Schöberl, R. Pippan, C. Motz, G. Dehm, A comparative micro-cantilever study of the mechanical behavior of silicon based passivation films, Thin Solid Films 518 (2009) 247–256, https://doi.org/10.1016/j.tsf.2009.07.143.

[9] J. Schaufler, C. Schmid, K. Durst, M. Göken, Determination of the interfacial strength and fracture toughness of a-C:H coatings by in-situ microcantilever bending, Thin Solid Films 522 (2012) 480–484, https://doi.org/10.1016/j.tsf.2012.08.031.

[10] D.E.J. Armstrong, A.S.M.A. Haseeb, S.G. Roberts, A.J. Wilkinson, K. Bade, Nanoindentation and micro-mechanical fracture toughness of electrodeposited nanocrystalline Ni-W alloy films, Thin Solid Films 520 (2012) 4369–4372, https://doi.org/10.1016/j.tsf.2012.02.059.

[11] R. Daniel, M. Meindlhumer, W. Baumegger, J. Zalesak, B. Sartory, M. Burghammer, C. Mitterer, J. Keckes, Grain boundary design of thin films: using tilted brittle interfaces for multiple crack deflection toughening, Acta Mater. 122 (2017) 130–137, https://doi.org/10.1016/j.actamat.2016.09.027.

[12] M.G. Mueller, G. Žagar, A. Mortensen, Stable room-temperature micron-scale crack growth in single-crystalline silicon, J. Mater. Res. 32 (2017) 3617–3626, https://doi.org/10.1557/jmr.2017.238.

[13] V. Schnabel, B.N. Jaya, M. Köhler, D. Music, C. Kirchlechner, G. Dehm, D. Raabe, J.M. Schneider, Electronic hybridisation implications for the damage-tolerance of thin film metallic glasses, Sci. Rep. 6 (2016) 1–12, https://doi.org/10.1038/srep36556.

[14] G. Žagar, V. Pejchal, M.G. Mueller, L. Michelet, A. Mortensen, Fracture toughness measurement in fused quartz using triangular chevron-notched micro-cantilevers, Scr. Mater. 112 (2016) 132–135, https://doi.org/10.1016/j.scriptamat.2015.09.032.

[15] S. Brinckmann, C. Kirchlechner, G. Dehm, Stress intensity factor dependence on anisotropy and geometry during micro-fracture experiments, Scr. Mater. 127 (2017) 76–78, https://doi.org/10.1016/j.scriptamat.2016.08.027.

[16] B. Merle, M. Göken, Fracture toughness of silicon nitride thin films of different thicknesses as measured by bulge tests, Acta Mater. 59 (2011) 1772–1779, https://doi.org/10.1016/j.actamat.2010.11.043.

[17] J. Pittari, G. Subhash, J. Zheng, V. Halls, P. Jannotti, The rate-dependent fracture toughness of silicon carbide- and boron carbide-based ceramics, J. Eur. Ceram. Soc. 35 (2015) 4411–4422, https://doi.org/10.1016/j.jeurceramsoc.2015.08.027.

[18] B. Gludovatz, S. Wurster, A. Hoffmann, R. Pippan, Fracture Toughness of Polycrystalline Tungsten Alloys, 12th Int. Conf. Fract. 2009, ICF-12, 7, 2009 5365–5372, https://doi.org/10.1016/j.ijrmhm.2010.04.007.

[19] J. Ast, M. Göken, K. Durst, Size-dependent fracture toughness of tungsten, Acta Mater. 138 (2017) 198–211, https://doi.org/10.1016/j.actamat.2017.07.030.

[20] C. Bohnert, N.J. Schmitt, S.M. Weygand, O. Kraft, R. Schwaiger, Fracture toughness characterization of single-crystalline tungsten using notched micro-cantilever specimens, Int. J. Plast. 81 (2016) 1–17, https://doi.org/10.1016/j.ijplas.2016.01.014.

[21] R.W. Margevicius, J. Riedle, P. Gumbsch, Fracture toughness of polycrystalline tungsten under mode I and mixed mode I/II loading, Mater. Sci. Eng. A 270 (1999) 197–209, https://doi.org/10.1016/S0921-5093(99)00252-X.

[22] V. Nikolic, S. Wurster, D. Firneis, R. Pippan, Improved fracture behavior and microstructural characterization of thin tungsten foils, Nucl. Mater. Energy. 9 (2016) 181–188, https://doi.org/10.1016/j.nme.2016.06.003.

[23] ASM Handbook, Volume 2, Properties and Selection: Nonferrous Alloys and Special-purpose Materials, 1998 https://doi.org/10.1007/s004310050884.

[24] ASTM E399-09, Standard Test Method for Plane-strain Fracture Toughness KIC of Metallic Materials, ASTM Int., West Conshohocken, PA, 2009 https://doi.org/10.1520/E0399-09 2009.

[25] ASTM, E1820-01, Standard Test Method for Measurement of Fracture Toughness, ASTM Int, West Conshohocken, PA, 2003 https://doi.org/10.1520/E1820-01.

[26] J. Ast, M. Ghidelli, K. Durst, M. Göken, M. Sebastiani, A.M. Korsunsky, A review of experimental approaches to fracture toughness evaluation at the micro-scale, Mater. Des. 173 (2019), 107762. https://doi.org/10.1016/j.matdes.2019.107762.

[27] X.K. Zhu, J.A. Joyce, Review of fracture toughness (G, K, J, CTOD, CTOA) testing and standardization, Eng. Fract. Mech. 85 (2012) 1–46, https://doi.org/10.1016/j.engfracmech.2012.02.001.

[28] S. Wurster, C. Motz, R. Pippan, Characterization of the fracture toughness of micro-sized tungsten single crystal notched specimens, Philos. Mag. 92 (2012) 1803–1825, https://doi.org/10.1080/14786435.2012.658449.

[29] J. Ast, T. Przybilla, V. Maier, K. Durst, M. Göken, Microcantilever bending experiments in NiAl - evaluation, size effects, and crack tip plasticity, J. Mater. Res. 29 (2014) 2129–2140, https://doi.org/10.1557/jmr.2014.240.

[30] B.N. Jaya, S. Goto, G. Richter, C. Kirchlechner, G. Dehm, Fracture behavior of nano-structured heavily cold drawn pearlitic steel wires before and after annealing, Mater. Sci. Eng. A 707 (2017) 164–171, https://doi.org/10.1016/j.msea.2017.09.010.

[31] M. Alfreider, D. Kozic, O. Kolednik, D. Kiener, In-situ elastic-plastic fracture mechanics on the microscale by means of continuous dynamical testing, Mater. Des. 148 (2018) 177–187, https://doi.org/10.1016/j.matdes.2018.03.051.

[32] A. Kumar, A.K. Saxena, C. Kirchlechner, M. Herbig, S. Brinkmann, In situ study on fracture behaviour of white etching layers formed on rails, Acta Mater. 180 (2019) 60–72, https://doi.org/10.1016/j.actamat.2019.08.060.

[33] M.J. Pfeifenberger, M. Mangang, S. Wurster, J. Reiser, A. Hohenwarter, W. Pfleging, D. Kiener, R. Pippan, The use of femtosecond laser ablation as a novel tool for rapid micro-mechanical sample preparation, Mater. Des. 121 (2017) 109–118, https://doi.org/10.1016/j.matdes.2017.02.012.

[34] D.E.J. Armstrong, A.J. Wilkinson, S.G. Roberts, A.J. Wilkinson, S.G.R, Micro-mechanical Measurements of Fracture Toughness of Bismuth Embrittled Copper Grain Boundaries, 839, 2011 https://doi.org/10.1080/09500839.2011.573813.

[35] J. Ast, B. Merle, K. Durst, M. Göken, Fracture toughness evaluation of NiAl single crystals by microcantilevers—a new continuous J-integral method, J. Mater. Res. 31 (2016) 3786–3794, https://doi.org/10.1557/jmr.2016.393.

[36] F. Iqbal, J. Ast, M. Göken, K. Durst, In situ micro-cantilever tests to study fracture properties of NiAl single crystals, Acta Mater. 60 (2012) 1193–1200, https://doi.org/10.1016/j.actamat.2011.10.060.

[37] J. Ast, J.J. Schwiedrzik, J. Wehrs, D. Frey, M.N. Polyakov, J. Michler, X. Maeder, The brittle-ductile transition of tungsten single crystals at the micro-scale, Mater. Des. 152 (2018) 168–180, https://doi.org/10.1016/j.matdes.2018.04.009.

[38] A.K. Saxena, A. Kumar, M. Herbig, S. Brinckmann, G. Dehm, C. Kirchlechner, Micro fracture investigations of white etching layers, Mater. Des. 180 (2019), 107892. https://doi.org/10.1016/j.matdes.2019.107892.

[39] R. Soler, S. Gleich, C. Kirchlechner, C. Scheu, J.M. Schneider, G. Dehm, Fracture toughness of Mo₂BC thin films: intrinsic toughness versus system toughening, Mater. Des. 154 (2018) 20–27, https://doi.org/10.1016/j.matdes.2018.05.015.

[40] K. Matoy, H. Schönherr, T. Detzel, G. Dehm, Micron-sized fracture experiments on amorphous SiOx films and SiOx/SiNx multi-layers, Thin Solid Films 518 (2010) 5796–5801, https://doi.org/10.1016/j.tsf.2010.05.114.

[41] B. Philippi, K. Matoy, J. Zechner, C. Kirchlechner, G. Dehm, Fracture toughness of intermetallic Cu6Sn5 in lead-free solder microelectronics, Scr. Mater. 123 (2016) 38–41, https://doi.org/10.1016/j.scriptamat.2016.05.039.

[42] S. Brinckmann, K. Matoy, C. Kirchlechner, G. Dehm, On the influence of microcantilever pre-crack geometries on the apparent fracture toughness of brittle materials, Acta Mater. 136 (2017) 281–287, https://doi.org/10.1016/j.actamat.2017.07.014.

[43] C. Kirchlechner, J. Keckes, C. Motz, W. Grosinger, M.W. Kapp, J.S. Micha, O. Ulrich, G. Dehm, Impact of instrumental constraints and imperfections on the dislocation structure in micron-sized Cu compression pillars, Acta Mater. 59 (2011) 5618–5626, https://doi.org/10.1016/j.actamat.2011.05.037.

[44] D. Yin, C.J. Marvel, F.Y. Cui, R.P. Vinci, M.P. Harmer, Microstructure and fracture toughness of electrodeposited Ni-21 at.% W alloy thick films, Acta Mater. 143 (2018) 272–280, https://doi.org/10.1016/j.actamat.2017.10.001.

[45] R.H. Dodds, T.L. Anderson, M.T. Kirk, A framework to correlate a/W ratio effects on elastic-plastic fracture toughness (Jc), Int. J. Fract. 48 (1991) 1–22, https://doi.org/10.1007/BF00012499.